Spontaneous rhythmic field potentials of isolated mouse hippocampal–subicular–entorhinal cortices *in vitro*

C. P. Wu[1,5], H. L. Huang[1], M. Nassiri Asl[1], J. W. He[1], J. Gillis[1,3], F. K. Skinner[1,2,3,4,5] and L. Zhang[1,2,5,6]

[1]*Toronto Western Research Institute, University Health Network,* [2]*Department of Medicine, (Division of Neurology)* [3]*Department of Physiology,* [4]*Institute of Biomaterials and Biomedical Engineering,* [5]*Epilepsy Research Program and* [6]*Institute of Medical Science, University of Toronto, Toronto, Ontario, Canada M5T 2S8*

The rodent hippocampal circuit is capable of exhibiting *in vitro* spontaneous rhythmic field potentials (SRFPs) of 1–4 Hz that originate from the CA3 area and spread to the CA1 area. These SRFPs are largely correlated with GABA-A IPSPs in pyramidal neurons and repetitive discharges in inhibitory interneurons. As such, their generation is thought to result from cooperative network activities involving both pyramidal neurons and GABAergic interneurons. Considering that the hippocampus, subiculum and entorhinal cortex function as an integrated system crucial for memory and cognition, it is of interest to know whether similar SRFPs occur in hippocampal output structures (that is, the subiculum and entorhinal cortex), and if so, to understand the cellular basis of these subicular and entorhinal SRFPs as well as their temporal relation to hippocampal SRFPs. We explored these issues in the present study using thick hippocampal–subicular–entorhinal cortical slices prepared from adult mice. SRFPs were found to spread from the CA1 area to the subicular and entorhinal cortical areas. Subicular and entorhinal cortical SRFPs were correlated with mixed IPSPs/EPSPs in local pyramidal neurons, and their generation was dependent upon the activities of GABA-A and AMPA glutamate receptors. In addition, the isolated subicular circuit could elicit SRFPs independent of CA3 inputs. We hypothesize that the SRFPs represent a basal oscillatory activity of the hippocampal–subicular–entorhinal cortices and that the subiculum functions as both a relay and an amplifier, spreading the SRFPs from the hippocampus to the entorhinal cortex.

(Resubmitted 7 June 2006; accepted after revision 28 July 2006; first published online 3 August 2006)
Corresponding author L. Zhang: Room 13-411, Toronto Western Hospital, 399 Bathurst Street, Toronto, Ontario, Canada M5T 2S8. Email: liangz@uhnres.utoronto.ca

Several recent studies have demonstrated that the rodent hippocampal circuit is capable of exhibiting spontaneous population rhythmic activities *in vitro*. We have, for example, observed spontaneous rhythmic field potentials (SRFPs) of 1–4 Hz in whole hippocampal isolates (Wu *et al.* 2002) and in thick (1 mm) hippocampal slices of mice (Wu *et al.* 2005*a*,*b*). Others have shown spontaneous field rhythms of 2–3 Hz in conventional ventral (but not dorsal) hippocampal slices of rats and mice (Papatheodoropoulos & Kostopoulos, 2002; Maier *et al.* 2002, 2003; Kubota *et al.* 2003; Colgin *et al.* 2004). Although named differently, these spontaneous population rhythmic activities share some common features: (1) they originate from the CA3 circuit; (2) they persist in standard *in vitro* conditions without extra ionic/pharmacological manipulation or excessive afferent stimulation; (3) they are correlated largely with GABA-A IPSPs in pyramidal neurons; and (4) they are abolished by GABA-A or AMPA (but not NMDA) glutamate receptor antagonists. As such, the generation of these population rhythmic activities is thought to result from cooperative network activities involving GABAergic inhibitory interneurons (Wu *et al.* 2002, 2005*a*,b).

These spontaneous population rhythmic activities have been shown to be involved in hippocampal synaptic plasticity and circuit development. Colgin *et al.* (2004) have explored the relationship between spontaneous field rhythms (∼2 Hz) and long-term potentiation (LTP) in the CA1 area of conventional rat ventral hippocampal slices. Their data show that CA1 LTP is weak or absent in slices exhibiting the spontaneous field rhythm but can be uncovered after severing the Schaffer collateral projection and hence eliminating the CA1 spontaneous field rhythm. It is hypothesized that this spontaneous field rhythm constitutes an intrinsic mechanism that regulates memory-related synaptic plasticity. We have examined the postnatal development of the SRFPs in mouse hippocampal isolates (Wong *et al.* 2005). Our data show that SRFPs start to emerge in mouse

 DOI: 10.1113/jphysiol.2006.114918

hippocampal isolates around postnatal day 10, stabilize after postnatal day 15 and persist into adulthood. The postnatal development of SRFPs is in parallel with age-dependent modifications in the morphological and electrophysiological properties of rodent hippocampal neurons (cf. Wong *et al.* 2005), probably participating in activity-dependent consolidation processes of developing hippocampal networks. To demonstrate further the physiological significance of hippocampal SRFPs, in the present study we address the following issues: (1) whether the subiculum and entorhinal cortex (EC) exhibit similar SRFPs; (2) if so, what is the cellular basis of subicular and EC SRFPs; and (3) what is the temporal relation between hippocampal and subicular/EC SRFPs.

The subiculum and EC are the main output structures of the hippocampus. Subicular pyramidal neurons receive abundant axonal projections from CA1 pyramidal neurons, and the axons of subicular pyramidal neurons project into the EC and adjacent areas (Amaral & Witter, 1989; Lavenex & Amaral, 2000). The hippocampus, subiculum and EC function as an integrated system that is crucial for learning and memory processes (Naber *et al.* 2000; O'Mara *et al.* 2001; Battaglia *et al.* 2004; Squire *et al.* 2004; O'Mara, 2005), and abnormalities in this system have been implicated in pathological processes of Alzheimer's disease (Flood, 1991; Anderton *et al.* 1998), schizophrenia (Gray *et al.* 1991; Greene, 1996; Harrison, 2004) and temporal lobe epilepsy (Cohen *et al.* 2002; Wozny *et al.* 2003; Knopp *et al.* 2005). Whereas information is accumulating regarding the morphological and electrophysiological properties of individual neurons and pharmacologically induced rhythmic activities (Finch *et al.* 1983, 1988; Behr *et al.* 1996; Mason, 1993; Stewart & Wong, 1993; Greene & Totterdell, 1997; Colling *et al.* 1998; D'Antuono *et al.* 2001; Menendez de la Prida *et al.* 2003; Menendez de la Prida & Gal, 2004) in the subicular and EC areas, much less is known about the intrinsic network activities of the integrated hippocampal–subicular–EC circuits. It is therefore of interest to establish an *in vitro* model for further investigation of this issue.

We thus produced thick hippocampal–subicular–EC slices from adult mice and monitored regional rhythmic activities via extracellular and whole-cell patch recordings. Our data show that the SRFPs spread from CA3 towards the EC area and that the intrinsic rhythmicity of the subicular circuit plays a key role in spreading the SRFPs from the hippocampus to the EC. The present data have been presented previously in abstract form (Zhang *et al.* 2005).

Methods

C57Bl/6 mice (21 days to 3 months of age) were used in the present experiments. All experiments conducted in this study have been reviewed and approved by the Animal Care Committee of Toronto Western Research Institute, University Health Network, according to the standard operating procedures, which conform to the requirements of the Animals for Research Act and the Canadian Council on Animal Care Guidelines. Only a minimal and necessary number of animals were used in this study. General procedures for slice preparation, *in vitro* perfusion, electrophysiological recordings and data analyses have been previously described (Wu *et al.* 2002, 2005*a*,*b*).

Slice preparation and *in vitro* perfusion

The animal was deeply anaesthetized with isoflurane and then decapitated. The brain was quickly removed, hemi-sectioned and immersed in an ice-cold, oxygenated artificial cerebrospinal fluid (ACSF) for 4–5 min before further dissection. The brainstem–thalamus tissues were then removed to expose the dorsal (or dentate gyrus) side of the hippocampus. Because the hippocampal fissure structurally divides the dentate gyrus and the CA2/CA1 areas, we applied a fine glass probe along the hippocampal fissure and gently separated the dentate gyrus from the CA2/CA1 areas while keeping dentate gyrus–CA3 connections. We then glued the brain tissue onto an aluminium block and obtained vibrotome slices along the hippocampal transverse plane. The thickness of slices was 1 mm for dorsal hippocampal–cortical sections and 0.7–0.8 mm for ventral sections because the CA3/CA1 striatum radiatum areas of the ventral hippocampus are wider (or thicker) than those in the dorsal hippocampus. After slicing, we separated hippocampal and adjacent cortical tissues along the lateral ventricle, and made a surgical cut near the rhinal fissure to produce S-shaped tissue pieces that encompassed the dentate gyrus, CA3, CA1 and subicular and EC areas (Fig. 1*A* and 1*B*). The thick hippocampal–EC slices were stabilized in an oxygenated (95% O_2–5% CO_2) ACSF at 32–33°C for 1–6 h before recordings. For recordings, the slice was placed in a submerged chamber and perfused with the oxygenated ACSF at 32–33°C. The perfusion rate was $\sim$15 ml min^{-1}, and both top and bottom sides of the thick slice were effectively perfused in our recording chamber (see Wu *et al.* 2002 for a detailed description of our perfusion apparatus). The ACSF contained (mM): NaCl 125, KCl 3.5, NaH_2PO_4 1.25, $NaHCO_3$ 25, $CaCl_2$ 2, $MgSO_4$ 1.3 and glucose 10.

To produce miniature slices, we prepared thick slices as described and then surgically isolated dentate gyrus–CA3 areas, CA1-subicular areas or the subicular area alone. These surgical incisions were made immediately after slicing and miniature slices were allowed to stabilize in the oxygenated ACSF at 32–33°C for $\geq$ 2 h before recordings in an attempt to minimize incision-associated disturbance of neuronal activities.

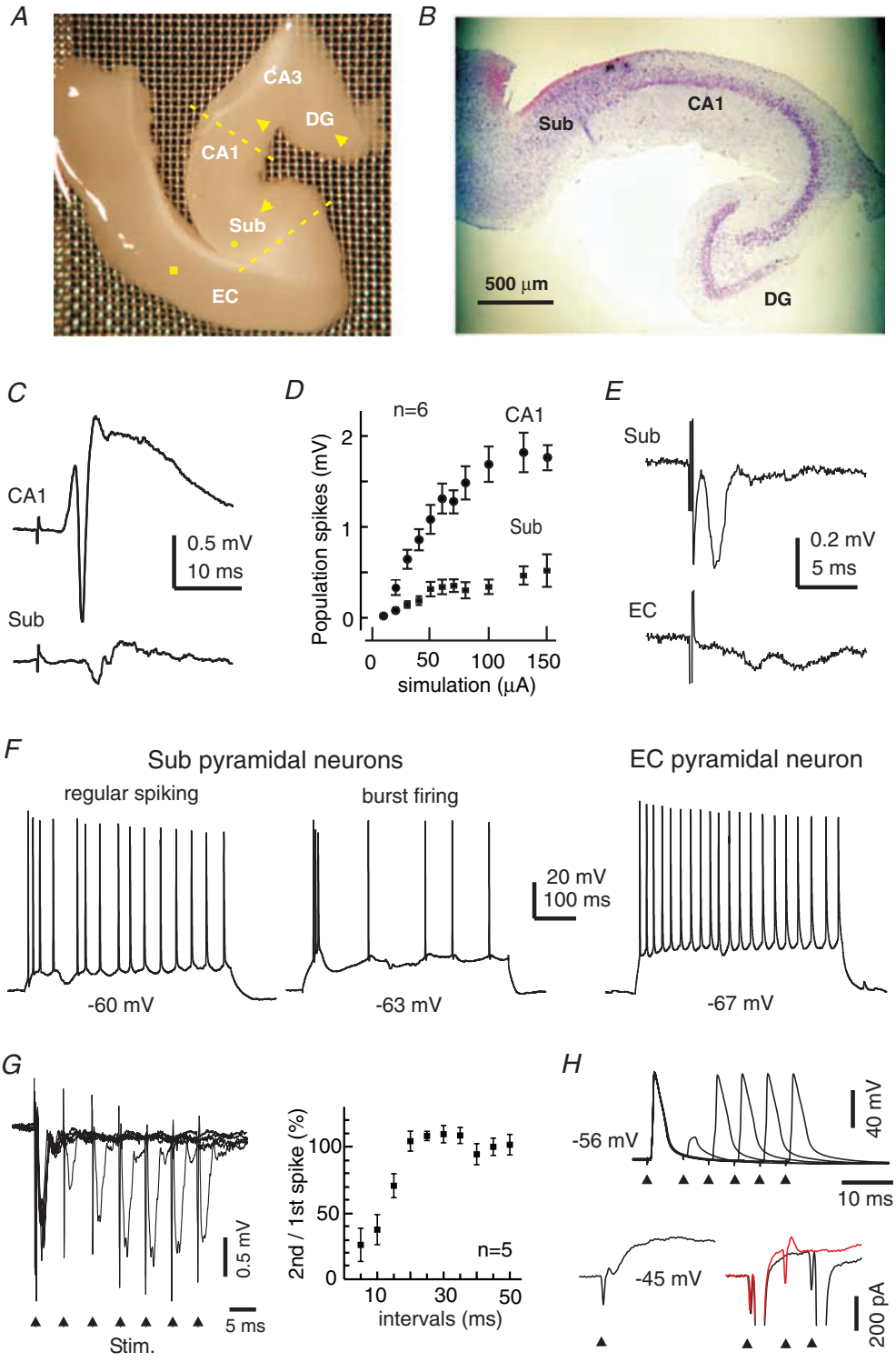

Figure 1. Basic electrophysiological properties of thick hippocampal–subicular–EC slices
A, a photo taken from a freshly prepared thick slice. Yellow dashed lines indicate the positions at which surgical cuts can be made to produce miniature CA1–subicular slices. Arrowheads show the position of a bipolar stimulating electrode used to stimulate the perforant pathway, Schaffer collateral pathway or subicular–EC projection pathway. The filled circle or square denotes the position of the stimulating electrode for evoking subicular population spikes or evoking EC field potentials, respectively. Sub, subiculum; EC, entorhinal cortex; DG, dentate gyrus. *B*, a representative section (15 μm thickness) was obtained from a fixed thick slice and stained with cresyl violet. *C*, CA1 and subicular synaptic field potentials were evoked by stimulating the dentate gyrus area. Illustrated traces

In some experiments, we prepared conventional coronal slices (0.5 mm thickness, two slices per half brain) by vibrotome cuts from whole-brain chunks. These coronal slices contained ventral CA1/subicular and adjacent EC tissues but excluded CA2/CA3 areas (see Fig. *9A*). These conventional slices were similarly maintained as described for the thick slices.

Electrophysiological recordings and afferent stimulation

Glass electrodes (thin walled pipettes, 1.5 mm outside diameter, World Precision Instrument, Sarasota, FL, USA) were used for extracellular recordings. These electrodes were filled with a solution containing 150 mM NaCl and 2 mM HEPS (pH 7.4; resistance, ∼2 MΩ). Field potentials were recorded via a dual-channel amplifier (700A, Axon Instruments, Union City, CA, USA) and/or an extracellular recording amplifier (Model 300, AM Systems Inc., Carlsborg, WA, USA). The input frequency band of these amplifiers was set between DC and 3 kHz. Extracellular signals were further amplified (1000–5000 ×) before digitization (Digidata 1200 or 1300, Axon Instruments).

Patch electrodes were pulled from the thin walled glass pipettes and filled with a solution containing (mM): potassium gluconate 140, KCl 10, Hepes 2 and EGTA 0.1 (pH 7.25). The resistance of patch electrodes was 4–5 MΩ after being filled with the above solution. A 'blind' approach was used to search individual neurons in thick slices (Wu *et al.* 2005*a*,*b*).

O_2-sensitive carbon fibre microelectrodes and a polarographic amplifier (Chemical Microsensor 1201, Diamond General, Ann Arbor, MI, USA) were used to measure tissue O_2 levels in perfused slices (Wu *et al.* 2005*a*). These carbon fibre electrodes were calibrated in ACSF (at ∼32°C) that was aerated with 95% N_2–5% CO_2, 25% O_2–5% CO_2–70% N_2, 50% O_2–5% CO_2–45% N_2 or 95% O_2–5% CO_2. The output signals of the carbon fibre electrodes displayed a linear relation with the percentages of oxygen used for aerating the ACSF ($r \geq 0.95$, linear regression analysis). As oxygen aeration was increased from 5% to 95%, the corresponding net increases in the O_2 signals of these carbon fibre electrodes were in the range of 250–380 mmHg. The O_2 levels measured from different depths of thick slices displayed an asymmetric 'U' shaped profile; that is, higher O_2 levels at the top and bottom layers of the thick slices and the lowest O_2 level in the middle layer of the slices. Such a 'U' shaped O_2–depth profile is suggestive of effective perfusion of both top and bottom sides of the thick slice (see Wu *et al.* 2005*a*,*b*). The lowest O_2 levels (middle layer) were 42.5 ± 10.3 mmHg for subicular areas and 66.0 ± 16.5 mmHg for EC areas ($n = 10$ and 4 slices, respectively). These observations are in keeping with our previous measurements in the CA3/CA1 areas (Wu *et al.* 2005*a*,*b*), indicating adequate oxygenation of thick hippocampal–subicular–EC slices under our experimental conditions.

We used a bipolar tungsten wire electrode (diameter, 50 μm) for afferent stimulation. Constant current pulses (0.1–0.2 ms, 20–150 μA) were generated every 30 s by a Grass stimulator (S88) and delivered through an isolation unit. The stimulating electrode was placed in the dentate middle molecular layer, CA2 or subicular stratum radium area to stimulate the perforant pathway, Schaffer collateral pathway or subicular–EC projection pathway (arrowheads in Fig. 1*A*). For antidromic stimulation of subicular neurons, we placed the stimulating electrode in subicular alveus areas (circle in Fig. 1*A*). For EC stimulation, we placed the stimulating electrode in the medial EC area (square in Fig. 1*A*) in an attempt to activate a large number of medial EC cortical neurons. We routinely evoked CA1 synaptic field potentials as a functional indication of successfully prepared thick slices. The slices were excluded from the present data analyses if they did not exhibit stable synaptic field potentials or if their CA1 field EPSPs were ≤ 0.5 mV following near maximal (100–150 μA) stimulation of the perforant pathway or the Schaffer collateral pathway.

Data analyses

Evoked synaptic field potentials and basic intracellular parameters were measured as previously described (Zhang

were averaged from five consecutive measurements. *D*, the amplitudes (mean ± S.E.M.) of CA1 and subicular population spikes were plotted against the strengths of dentate gyrus stimulation (constant current pulses of 0.1 ms and 20–150 μA). *E*, subicular and EC (deep layer) field potentials evoked by stimulating the subicular area; illustrated traces were averaged from five consecutive responses. *F*, intracellular traces were collected from two subicular pyramidal neurons and an EC deep layer pyramidal neuron at indicated resting potentials. Repetitive discharges were evoked by intracellular injections of depolarizing current pulses of 300–500 pA. *G*, subicular population spikes were evoked by paired stimuli (arrowheads) in a thick slice. The amplitude ratios (mean ± S.E.M.) of the second/first population spikes were calculated from five slices and plotted against interstimulus intervals. *H*, intracellular traces were collected from a subicular pyramidal neuron at indicated membrane potentials. Top trace, voltage responses were evoked by paired stimuli at different interstimulation intervals. Bottom trace, currents were evoked by a subthreshold stimulus (left) and super-threshold stimuli at two intervals (right). The spike currents (right) were truncated for illustration purposes. Note the lack of spike current following the second stimulus when applied ∼7 ms after the first stimulus (red trace).

et al. 1994, 1995, 1998; Wu *et al.* 2002, 2005*a*,*b*). To calculate the reversal potential of SRFP-correlated synaptic currents, pyramidal neurons were voltage-clamped at different voltages (−40 to −70 mV). The charge transfer of SRFP-correlated synaptic currents (pC) was measured from ≥ 30 consecutive events at each holding voltage. The mean values of these measurements were plotted against holding voltages and fitted with a linear regression function ($r \geq 0.90$). The voltage at which the calculated linear regression line intersected the zero current level was taken as the reversal potential of SRFP-correlated synaptic currents. Spectral analyses were conducted using Micro-Origin (version 6, Origin Laboratory Corporation, Northampton, MA, USA) or pCLAMP software (version 9, Axon Instruments). To reduce the DC shift and high-frequency noise, original data were treated with a band-pass filter (0.2–0.5 Hz to 1000 Hz). Time–frequency analyses (Akay, 1997) of spontaneous field potentials were made from 65 s extracellular data segments, and the time resolution of these analyses was 0.5 s (Wu *et al.* 2005*a*). Statistical significance was determined using Student's *t* test or one-way ANOVA (SigmaStat or Origin). Mean and S.E.M. are presented throughout the text except where indicated.

Chemical and pharmacological agents

All solutions were made with deionized distilled water (specific resistance, 18.2 MΩ cm^{-1}; Milli-Q system). D-2-Amino-5-phosphopentanoate (AP5), 6-cyano-7-nitroquinoxaline-2,3-dione (CNQX) and bicuculline methiodide were purchased from Research Biochemicals Inc. (Canada).

Results

Basic electrophysiological properties of thick hippocampal–subicular–EC slices

Simultaneous extracellular recordings from the CA1 and subicular areas revealed stable synaptic field potentials following single stimulation of the dentate gyrus area (Fig. 1*C*). These field potentials displayed a typical stimulation strength-dependent increase in amplitude (Fig. 1*D*), and the CA1 and subicular population spikes were 1.2 ± 0.1 and 0.3 ± 0.03 mV ($n = 13$ slices), respectively, in response to near maximal dentate gyrus stimulation (current pulses of 100–150 μA). EC synaptic field potentials were reliably induced by stimulation of the CA1 or subicular area (Fig. 1*E*). Following subicular stimulation, the amplitudes of subicular population spikes and EC deep layer field EPSPs were 0.80 ± 0.19 and 0.32 ± 0.08 mV ($n = 16$), respectively.

Intracellular activities of subicular and EC pyramidal neurons were examined via whole-cell patch recordings. The basic intracellular parameters of subicular pyramidal neurons were: resting potential, −59.5 ± 0.8 mV; input resistance, 84.3 ± 5.5 MΩ; action potential amplitude, 95.4 ± 1.9 mV; and action potential half-width, 1.05 ± 0.05 ms ($n = 40$). The intracellular parameters of EC deep layer (V–VI) pyramidal neurons were: resting potential, −63.6 ± 0.6 mV; input resistance, 148.5 ± 7.6 MΩ; action potential amplitude, 96.9 ± 1.5 mV; and action potential half-width, 1.62 ± 0.14 ms ($n = 44$). Five pyramidal neurons were recorded from EC superficial layers (I–II) with: resting potential, −66.5 ± 3.2 mV; input resistance, 76.8 ± 8.8 MΩ; action potential amplitude, 95.3 ± 5.7 mV; and action potential half-width, 1.7 ± 0.37 ms. Generally, these measurements are in agreement with previous studies in conventional slices (Funahashi & Stewart, 1997; Mattia *et al.* 1997; Schmitz *et al.* 1998; Staff *et al.* 2000; Menendez de la Prida *et al.* 2003).

Previous studies have indicated that rat subicular pyramidal neurons exhibit two types of discharge patterns in response to intracellular stimulation: regular spiking and burst firing (Mattia *et al.* 1997; Staff *et al.* 2000; Menendez de la Prida *et al.* 2003). The burst firing is generally featured with a cluster of action potentials at frequencies of ∼200 Hz and is thought to result from high voltage-activated Ca^{2+} currents (Jung *et al.* 2001; but see Mattia *et al.* 1997). In our experiments, mouse subicular pyramidal neurons of thick slices also exhibited two types of discharge patterns following intracellular stimulation (depolarizing current pulses of 200–500 pA, 0.5–1 s). The burst firing was recognized by two to three spikes occurring in the first 200 ms of depolarizing pulses and the interspike intervals were ≤ 8 ms (Fig. 1*F*, middle trace). Of the 40 subicular pyramidal neurons recorded, 28 (70%) were considered as burst firing neurons, and the first and second interspike interval of the burst firing were 5.58 ± 0.31 and 6.90 ± 0.40 ms, respectively. The remaining 12 pyramidal neurons were considered as the regular spiking type (Fig. 1*F*, left-hand trace), and they discharged with evident spike adaptation but without early bursting firing. In response to intracellular injections of depolarizing current pulses, pyramidal neurons of EC deep and superficial layers discharged with evident spike adaptation but without bursting firing (Fig. 1*F*, right-hand trace).

To examine paired-pulse inhibition (Kapur *et al.* 1989) of the subicular circuit, we evoked antidromic subicular population spikes (see Methods) by identical twin stimuli with the interstimulus intervals varying from 5 to 50 ms (see Methods). As the twin stimuli were delivered at intervals of 5–10 ms, the second population spikes were greatly decreased as compared with the corresponding first population spikes (Fig. 1*G*). Similar paired-pulse inhibition was observed from individual subicular pyramidal neurons ($n = 5$). One example is

shown in Fig. 1*H* (top trace), where the first stimulus consistently induced action potentials with little variability in spike onset. The second stimulus, when applied ∼7 ms after the first stimulus, induced only a partial spike, which probably reflected an axon initial segment potential. When voltage-clamped at depolarizing potentials (−45 mV), this pyramidal neuron exhibited a large IPSC following a subthreshold or supra-threshold stimulus. The second supra-threshold stimulus, when applied near the peak of the evoked IPSC (∼6 ms after the first stimulus), was unable to evoke a spike current (Fig. 1*H*, bottom trace). In five of five subicular pyramidal neurons examined, the second supra-threshold stimulus failed to elicit an action potential or spike current when it was applied < 10 ms after the first stimulus. The IPSCs evoked by single subthreshold stimulation were 200–400 pA in amplitude ($n = 3$ pyramidal neurons). These observations suggest that the local inhibitory circuit of subicular neurons (Menendez de la Prida, 2003) is functional in the thick hippocampal–subicular–EC slices, and that the subicular SRFPs presented below are not a consequence of disinhibition (Harris & Stewart, 2001*a*; Benini & Avoli, 2005).

Regional SRFPs

Multiple extracellular recordings revealed stable and coherent SRFPs in the CA3/CA1, subicular and EC areas of the thick slices. The frequencies of SRFPs varied within the range 0.5–4 Hz, with a mean frequency of 1.6 ± 0.2 Hz ($n = 23$ slices; Fig. 2*A*). The CA3/CA1 SRFPs displayed upward (positive) or downward (negative) waveforms when recorded from the striatum pyramidale or radiatum area, respectively. The waveforms of subicular SRFPs were largely downward, and upward SRFPs appeared only in the subicular alveus area. When recorded from CA and subicular alveus areas, the SRFPs were often superimposed with ripple-like oscillatory spike activities of 100–200 Hz. Because the appearance of such ripples was region-dependent and their intracellular correlates were not clearly identified (see also Wu *et al.* 2005*b*), we did not examine in detail the ripple-like oscillations in the present experiments.

The SRFPs recorded from EC deep layer areas were often biphasic, and their amplitudes (0.02–0.1 μV) were smaller than those recorded from the CA3/CA1 and subicular areas (0.05–0.3 mV). When EC deep and superficial layer areas were simultaneously monitored, SRFPs coherent with those in the CA1 or subicular area were detectable in the EC deep layers (V–VI) but not in the superficial layers (I–II) ($n = 5$ slices, Fig. 2*B*). Such a layer-specific appearance of EC SRFPs is in keeping with the axonal projection profile of subicular pyramidal neurons (Kloosterman *et al.* 2003). However, further studies using the analysis of current source density are necessary to characterize the regional distribution of EC SRFPs (de Villers-Sidani *et al.* 2004; Gnatkovsky & de Curtis, 2006).

As the onset times of SRFPs were often difficult to determine, we measured peak-to-peak time lags of regional SRFPs (≥ 60 consecutive events in each slice) in an attempt to explore their temporal relations. CA1 and subicular SRFPs exhibited a stable temporal relation and the peaks of CA1 SRFPs were time-advanced compared with corresponding subicular SRFP peaks in all slices examined ($n = 13$, mean lags varying from 6.3 ± 0.5 to 29.3 ± 0.9 ms). The subicular and EC SRFPs appeared to occur simultaneously, and their peak-to-peak time lags could not be reliably measured because the EC SRFPs were small and their peaks were often difficult to recognize even after substantial filtering of the original data.

To explore the temporal relation of subicular and EC SRFPs, we monitored regional rhythmic activities before and after a surgical cut that separated the subicular and EC recording sites. Coherent SRFPs remained in the CA1 and subicular areas after the cut but regular rhythmic field potentials were absent in the isolated EC area ($n = 4$ slices; Fig. 2*A*). These observations could not be explained solely by non-specific damage to the EC circuit because the isolated EC areas were responsive to local afferent stimulation and showed spontaneous but irregular field potentials (0.05–0.2 Hz, data not shown). The latter observation is in keeping with recent *in vitro* studies of guinea-pig and rat EC neurons (Dickson *et al.* 2003; Kano *et al.* 2005). Thus, although the EC circuit is able to generate spontaneous population activities in isolation, the EC SRFPs observed from the 'intact' thick slices are largely dependent upon the subicular inputs.

To explore the possible influences of subicular neuronal activities on CA3 SRFPs, we surgically removed the CA1, subicular and EC areas and produced dentate gyrus–CA3 miniature slices (see Methods). In five dentate–CA3 miniature slices successfully prepared (CA3 population spikes of 0.96 ± 0.18 mV), stable SRFPs of 1.23 ± 0.17 Hz were observed from the CA3 area and their waveforms were comparable to those seen in the thick hippocampal–subicular–EC slices (see above). Thus, the activities of subicular neurons may have little influence on the CA3 SRFPs in the thick hippocampal–subicular–EC slices.

SRFP-correlated intracellular activities

Simultaneous extracellular and whole-cell patch recordings were used to examine SRFP-correlated intracellular activities. The exact distance between these two recording sites could not be determined under our experimental conditions. We estimate that these recordings sites were 300–600 μm apart.

Subicular pyramidal neurons. When monitored at voltages near resting potentials (∼−60 mV), subicular

pyramidal neurons exhibited periodic EPSPs or mixed EPSPs/IPSPs in correlation with local SRFPs and the peak-to-peak time lags between SRFPs and corresponding EPSPs varied in the range 3–25 ms. In the majority (27 out of 40) of subicular pyramidal neurons examined, the SRFP-correlated IPSP component became dominant when monitored at depolarizing voltages (−50 to −40 mV). As these neurons were depolarized to discharge, these periodic IPSPs effectively arrested tonic discharges (Fig. 3*A*).

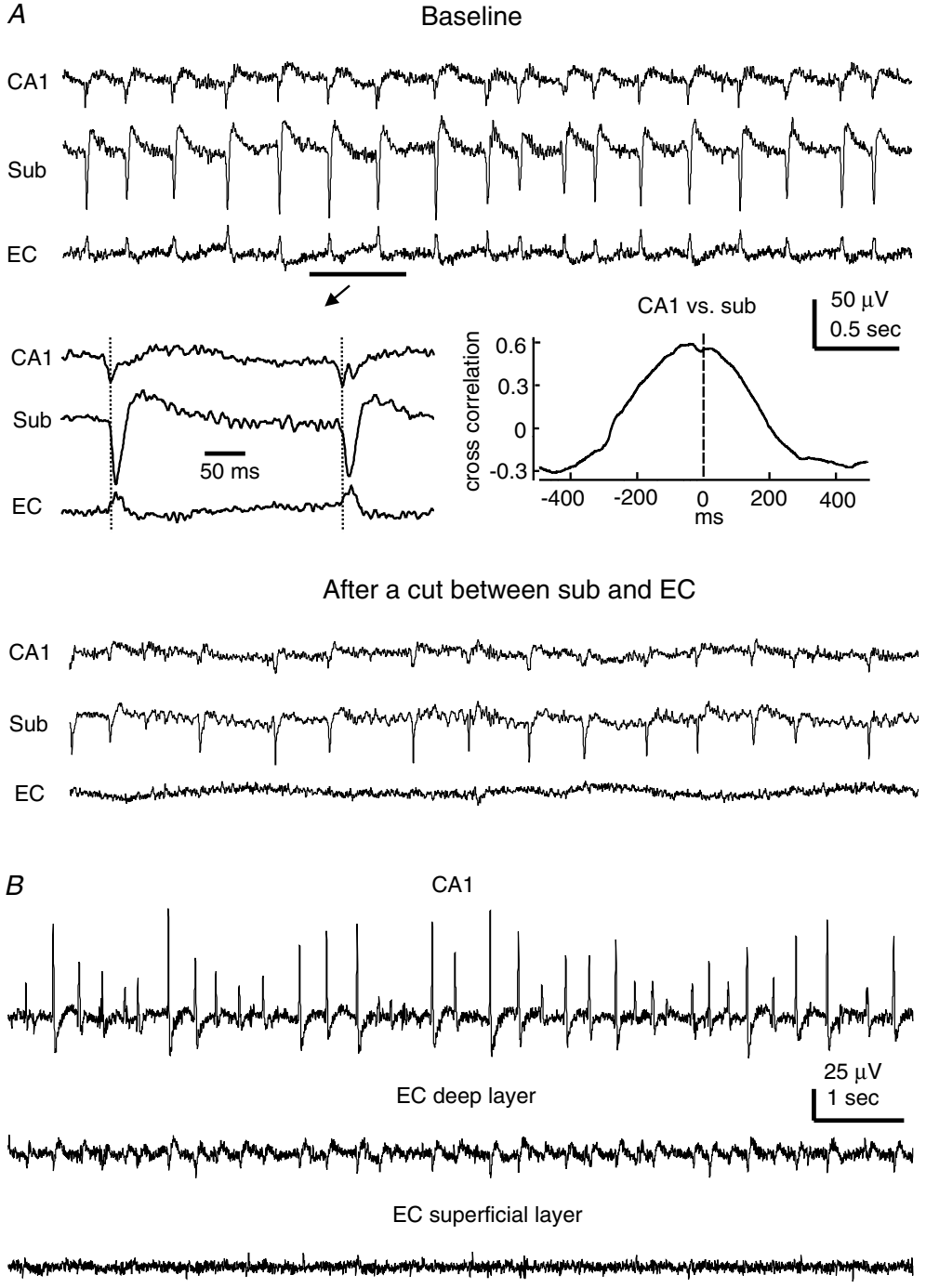

Figure 2. Regional SRFPs
A, extracellular traces were collected simultaneously from the CA1, subicular and EC deep layer areas of a thick slice. Top, baseline SRFPs. Middle, two representative SRFP events are shown in a fast sweep. A cross correlation plot was generated from five consecutive SRFP events including the two shown. Bottom, traces were collected ∼30 min after a surgical cut that separated the subicular and EC recording sites. *B*, extracellular traces were collected from an 'intact' thick slice, showing coherent SRFPs in CA1 and EC deep layer areas but not in the EC superficial layer area.

Monitored via voltage-clamp recordings at −60 to −40 mV, these neurons displayed mixed EPSCs/IPSCs in correlation with SRFPs, and the EPSC component often preceded the IPSC component (Fig. 3*B*). To estimate the reversal potential of SRFP-correlated synaptic currents, pyramidal neurons were voltage-clamped at different potentials (−70 to −40 mV) and the total charge transfer of these synaptic currents (pC) was plotted against holding potentials (see Methods). In 12 subicular pyramidal neurons examined, the estimated reversal potentials of SRFP-correlated synaptic currents were in the range of −43 to −65 mV, with a mean value of −54.2 ± 1.2 mV (Fig. 3*B*). Considering that our patch pipette solution and ACSF contained 10 mM Cl^- and 130.5 mM Cl^-, respectively (see Methods), such reversal potentials are suggestive of a Cl^--dominated ionic current (Zhang *et al.* 1991). Perfusions of thick slices with 10 μM bicuculline suppressed subicular SRFPs and

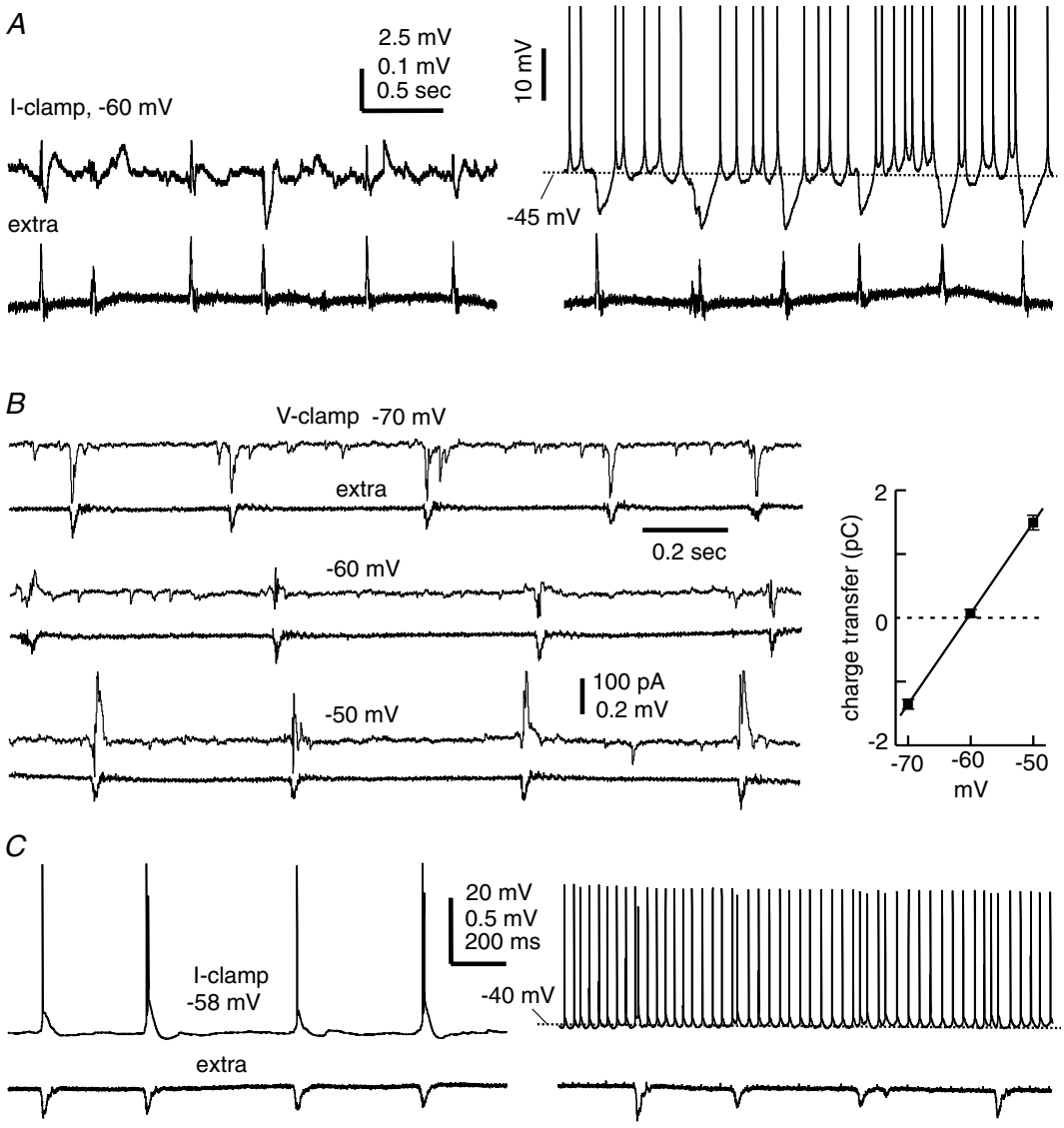

Figure 3. Intracellular correlates of subicular SRFPs
Data were obtained via simultaneous whole-cell recordings together with extracellular monitoring of local field potentials. *A*, voltage traces were collected from a subicular regular spiking pyramidal neuron at resting (∼−67 mV, right) and depolarized (∼−45 mV, left) potentials. Spike amplitudes in the right-hand traces were truncated for illustration purposes. *B*, current traces were collected from other regular spiking subicular pyramidal neuron at indicated different holding potentials. The charge transfer of SRFP-correlated synaptic currents (mean ± S.E.M. calculated from 30 consecutive events) was plotted against holding potentials. The line through data points was computed by a linear regression function ($r = 0.98$). *C*, voltage traces were collected from a burst firing subicular pyramidal neuron at resting (∼−58 mV, left) and depolarizing (∼−40 mV, right) potentials.

correlated intracellular activities and induced intermittent interictal-like discharges ($n = 4$, data not shown). Thus, the activities mediated by GABA-A receptors play a crucial role in the generation of subicular SRFPs.

Of the 40 pyramidal neurons examined, 13 neurons displayed only EPSPs/EPSCs in correlation with local SRFPs, even when monitored at −40 mV or more positive voltages (Fig. 3*C*). The lack of SRFP-correlated IPSP/IPSC components was unlikely to be due to a rundown of GABA-A receptor-mediated Cl^- currents because such a phenomenon was recognizable in 2–3 min after forming the whole-cell recordings. Moreover, when monitored via cell-attached voltage-clamp recordings prior to whole-cell dialysis, these neurons often exhibited SRFP-correlated spike currents. The burst firing subicular pyramidal neurons appeared to have a high tendency of exhibiting SRFP-correlated EPSPs. In the 13 pyramidal neurons that exhibited only SRFP-correlated EPSPs/EPSCs, 11 neurons were of the burst firing type. These observations raise an interesting issue regarding the specific role of burst firing subicular pyramidal neurons in the generation of local SRFPs (see Discussion).

EC deep layer pyramidal neurons. SRFP-correlated synaptic activities were observed in 32 of 44 EC deep layer pyramidal neurons examined. When monitored near resting potentials (−60 to −65 mV), these neurons exhibited EPSPs/EPSCs in correlation with SRFPs (Fig. 4*A*). Of the 32 recordings, SRFP-correlated IPSP/IPSC components were noticeable in 17 neurons when monitored at depolarizing voltages (−50 to −40 mV). These IPSPs/IPSCs were relatively small as compared with preceding EPSPs/EPSCs (Fig. 4*B*). The reversal potentials of SRFP-correlated synaptic currents (see Methods) were estimated from seven pyramidal neurons that exhibited relatively large IPSCs at −50 and −40 mV (Fig. 4*B*). These estimated reversal potentials varied in a range from −57 to −40 mV, with a mean value of -50.1 ± 2.4 mV. Thus, Cl^--dominated currents are a major component of the SRFP-correlated synaptic activities in some EC deep layer pyramidal neurons.

In 15 of the 32 EC deep layer neurons that exhibited SRFP-correlated synaptic activities, we observed only SRFP-correlated EPSPs/EPSCs (Fig. 4*C*) even when monitoring these neurons at −40 mV or more positive voltages. Perfusion of thick slices with 10 μM bicuculline suppressed the SRFPs and correlated intracellular activities and induced intermittent large-amplitude field potentials that were correlated with profound EPSPs/discharges in pyramidal neurons ($n = 3$, data not shown). Thus, although the EC SRFPs were not always correlated with evident IPSPs/IPSCs in local pyramidal neurons, the GABA-A receptor-mediated activities are necessary for the generation of EC SRFPs.

Five pyramidal neurons were recorded from EC superficial layer (I–II) areas. When monitored near −70 mV, these neurons exhibited spontaneous EPSPs/EPSCs (Fig. 4*D*) but these synaptic activities were not correlated with the SRFPs simultaneously recorded from the EC deep layer or subicular area.

Observations made by dual whole cell recordings. To explore further the dynamics of SRFP-correlated synaptic activities, we performed dual whole-cell recordings together with extracellular monitoring of subicular SRFPs. In paired recordings made from proximal (near CA2) CA1 pyramidal neurons and subicular pyramidal neurons ($n = 5$ pairs), the SRFP-correlated IPSCs in the CA1 neurons led those in corresponding subicular neurons (Fig. 5*C*). As measured from 30 consecutive coherent IPSCs from each pair, the time lags in the onsets of CA1 and subicular IPSCs were 4.5 ± 0.8, 7.3 ± 0.4, 7.5 ± 0.3, 9.1 ± 0.8 and 12.8 ± 0.3 ms, (Fig. 5*A*). These observations are in keeping with the peak-to-peak measurements of CA1 and subicular SRFPs presented above and further demonstrate that in 'intact' slices the SRFPs spread from CA3 towards the subicular area.

In three paired recordings made from subicular and EC deep layer pyramidal neurons, a consistent temporal relation between SRFP-correlated regional EPSCs was noticeable in one pair. In this case, the onset of subicular EPSCs was time advanced by 4.0 ± 0.2 ms in relation to EC EPSCs (Fig. 5*B*). In the other two pairs, the subicular and EC EPSCs were highly coherent but without a consistent temporal relation in their onsets (time lags of 1.8 ± 0.4 and 1.6 ± 0.5 ms, respectively). A clear temporal relation between subicular and EC neuronal activities became evident following perfusion of ∼1 μM bicuculline, which induced large amplitude rhythmic EPSPs or EPSPs/spikes in both subicular and EC pyramidal neurons. Under these conditions, the rising phases of EC EPSPs or EPSPs/spikes were delayed in relation to subicular EPSPs or EPSPs/spikes (Fig. 5*D*), suggesting a subicular-to-EC spread of excitatory activities in disinhibited thick slices. However, further experiments are needed to examine the temporal relation of SRFP-correlated synaptic activities between subicular and EC deep neurons.

Four paired whole-cell recordings were made from subicular pyramidal neurons. The SRFP-correlated EPSCs and/or IPSCs appeared to occur synchronously in these paired neurons without a clear time lag in their onsets (Fig. 5*B*). These observations suggest that subicular SRFPs are mediated by synchronized synaptic activities from a large population of pyramidal neurons. However, interneuronal synaptic connections were not evident in the paired neurons, as discharging one neuron by intracellular stimulation did not induce noticeable synaptic activities in the other corresponding neuron (Fig. 5*E*). Following perfusion of slices with 5–10 μM

bicuculline, these paired subicular neurons exhibited synchronous epileptiform discharges but still failed to display interneuronal synaptic connections as tested by intracellularly induced discharges (data not shown). Previous studies have indicated that only closely neighboured pyramidal neurons (≤ 20 or ≤ 50 μm apart in the CA1 or EC area) are capable of exhibiting interneuronal synaptic connections when recorded

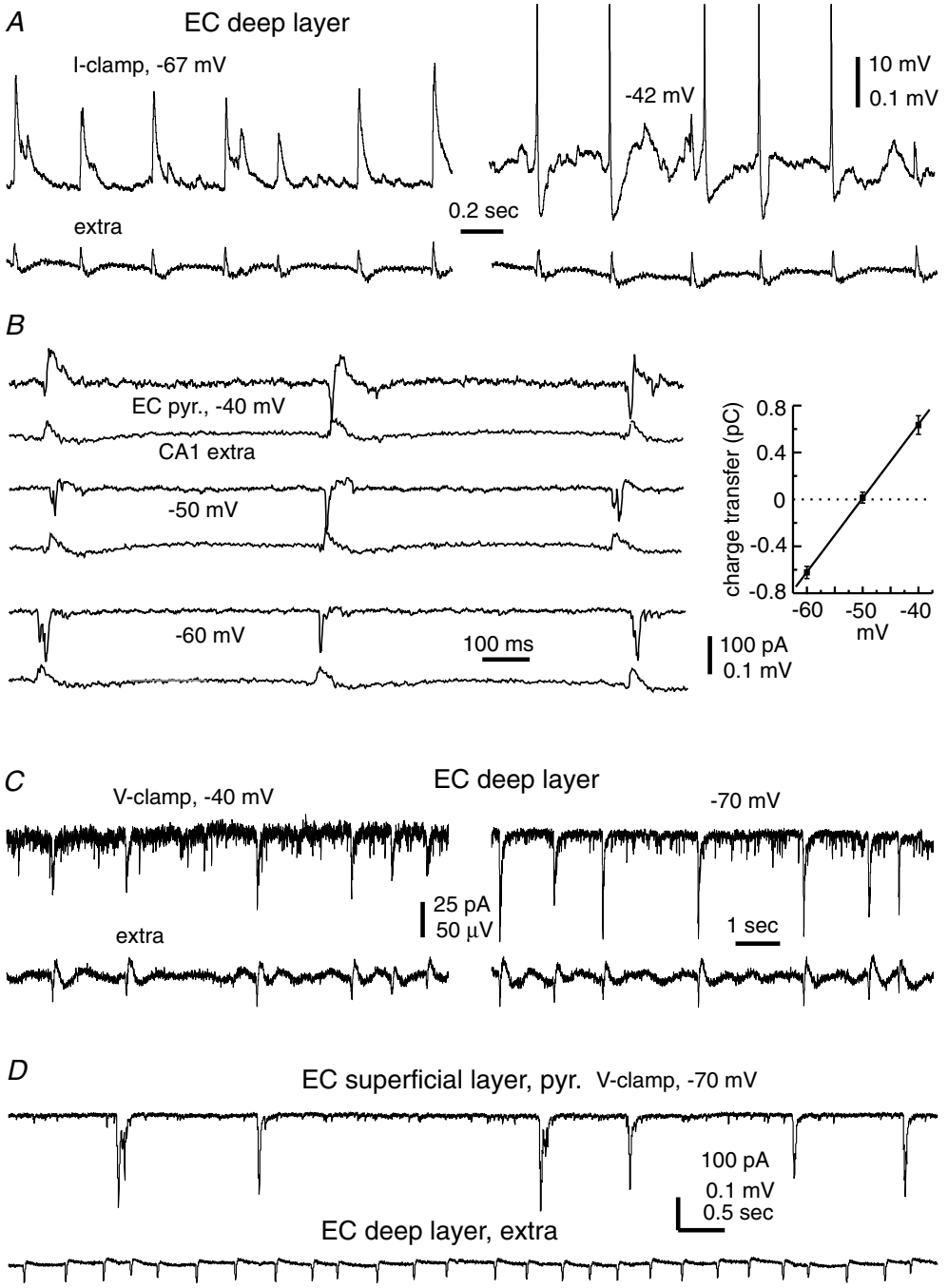

Figure 4. Intracellular correlates of EC SRFPs
Data were collected via simultaneous whole-cell recordings together with extracellular monitoring of field potentials. *A*, voltage traces were collected from an EC deep layer pyramidal neuron at resting (∼−67 mV, left) and positive (∼−42 mV, right) potentials. *B*, current traces were collected from another deep layer pyramidal neuron at indicated holding potentials. The charge transfer of SRFP-correlated synaptic currents (mean ± S.E.M. calculated from 30 consecutive events) was plotted against holding potentials. The line through data points was computed by a linear regression function ($r = 0.94$). *C*, current traces were collected from another EC deep layer pyramidal neuron at indicated holding potentials. *D*, current traces were collected from a superficial layer pyramidal neuron at −70 mV.

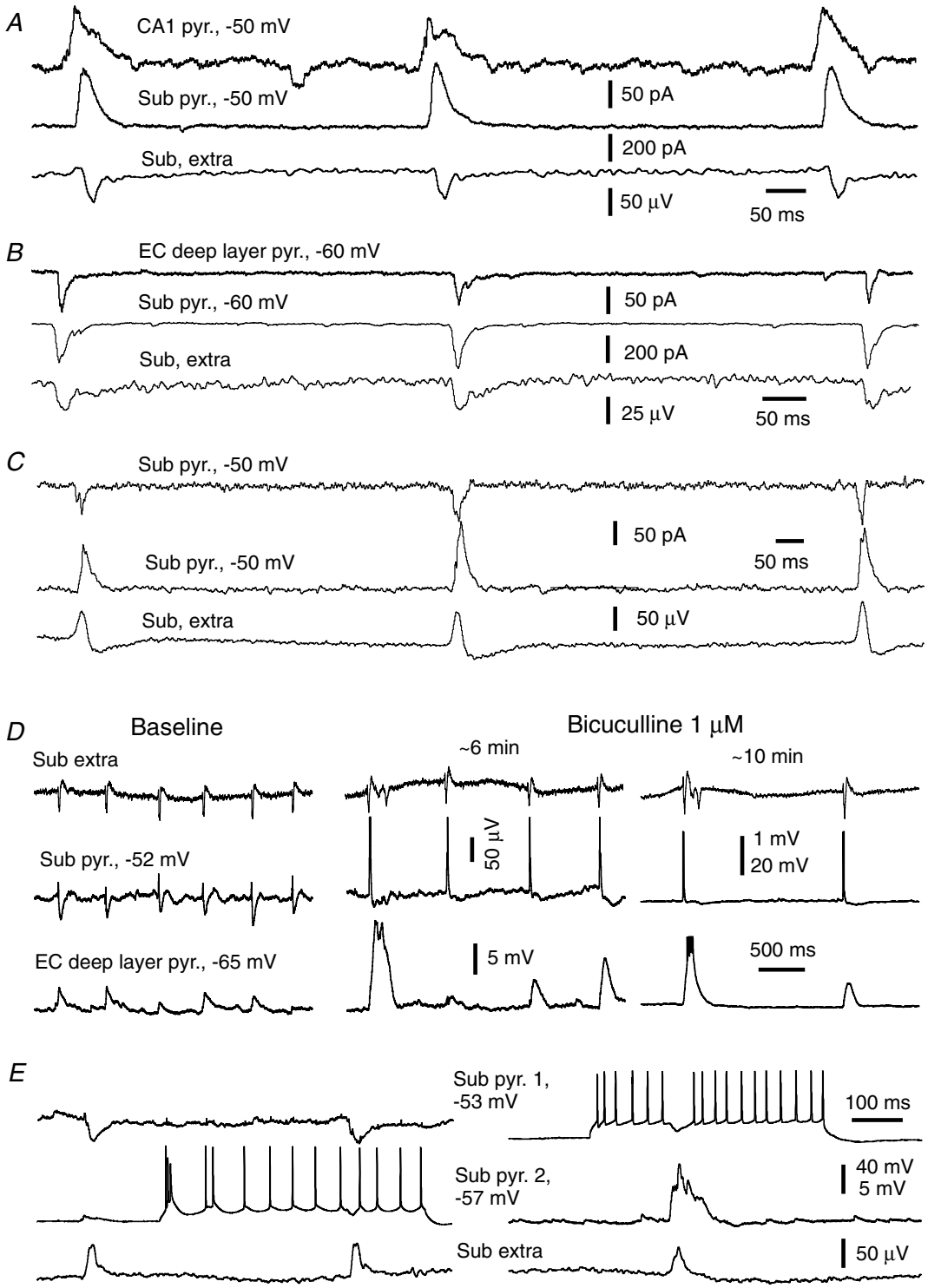

Figure 5. SRFP-correlated intracellular activities
Data were obtained via dual whole-cell recordings together with extracellular monitoring of subicular field potentials. *A–C*, representative current traces were collected at indicated holding potentials, and paired recordings were made from a subicular and a CA1 pyramidal neuron (*A*), from an EC deep layer and a subicular pyramidal neuron (*B*), and from two subicular pyramidal neurons (*C*). *D*, voltage traces were collected from a subicular pyramidal neuron and an EC deep layer pyramidal neuron during baseline recordings and following perfusion of ~1 μM bicuculline; initial resting potentials are indicated. *E*, voltage traces were collected from two subicular pyramidal neurons at indicated initial resting potentials. For each neuron, traces were presented at a low and high gain to show action potentials and synaptic potentials, respectively. Repetitive discharges were induced by intracellular injection of depolarizing currents (300 pA).

simultaneously via microelectrodes (Deuchars & Thomson, 1996; Dhillo & Jones, 2000). Our dual whole-cell recordings were made from subicular pyramidal neurons $\geq 300\,\mu$m apart, which probably rendered a low probability of observing interneuronal synaptic connections in our experiments. Thus, further experiments to record from closely neighboured subicular neurons and to assess their morphological features in thick slices are necessary to characterize the subicular circuit responsible for the generation of SRFPs.

SRFPs originate from isolated subicular circuit

To explore the intrinsic rhythmicity of the subicular circuit, we adopted a miniature slice preparation as previously described by Harris & Stewart (2001*b*). We first prepared the thick slices and then surgically removed the dentate gyrus–CA3 and EC tissues (as indicated by dashed lines in Fig. 1*A*) while keeping CA1 and subicular areas. CA1–subicular synaptic connections were preserved in these CA1–subicular miniature slices. Following local CA1 stimulation at near maximal intensities, CA1 and subicular population spikes were 2.8 ± 0.3 and 0.6 ± 0.1 mV, respectively ($n = 25$ slices). SRFPs were consistently observed from the subicular area of miniature slices. These SRFPs contained frequent, small-amplitude ($\leq 30\,\mu$V) components as compared with those seen in the 'intact' thick slices (with CA3/EC inputs). Spectrogram analyses reveal that subicular SRFPs with or without CA3/EC inputs differ markedly in their frequency distribution profiles. As seen in Fig. 6, the subicular SRFPs without CA3/EC inputs encompass more persistent high-frequency (> 10 Hz) activities, whereas the subicular SRFPs with CA3/EC inputs contain periodical high-frequency activities which render significant variability in mean frequency over time ($P < 0.05$ over 10 s intervals). Such variability is absent in the subicular SRFPs without CA3/EC inputs.

The subicular SRFPs observed from the CA1–subicular miniature slices (without CA3 input) were often, but not always, correlated with CA1 SRFPs (Fig. 7*A*). The overall frequency of subicular SRFPs (1.8 ± 0.1 Hz) was significantly higher than that of CA1 SRFPs (1.3 ± 0.1 Hz, $P = 0.013$, independent t test, $n = 23$ slices; Fig. 7*B*). Measurements of peak-to-peak time lags of regional SRFPs showed that the subicular SRFPs were time-advanced compared with CA1 SRFPs in a majority (19 of 23) of slices examined (Fig. 7*C*). After a surgical cut that further separated the CA1 and subicular recording sites, the subicular SRFPs were still detectable, although with decreased amplitudes and frequencies, whereas the isolated CA1 area showed no regular rhythmic activity ($n = 4$ slices; Fig. 7*D*). To further examine the intrinsic rhythmicity of the subicular circuit, we then prepared subiculum only miniature slices immediately after vibrotome sections (see Methods). In six subiculum only miniature slices successfully prepared, local afferent stimulation induced population spikes of 0.62 ± 0.10 mV and the frequencies of SRFPs were 0.63 ± 0.09 Hz. Collectively, these observations suggest that the subicular circuit is capable of generating SRFPs in isolation.

Subicular SRFPs were reversibly blocked by perfusions of miniature slices with a modified ACSF in which Mg^{2+} was increased from 1.3 to 6.3 mM while keeping the rest of the components constant ($n = 3$ slices, Fig. 8*A*). Perfusion of miniature slices with bicuculline or CNQX (each at $10\,\mu$M, 6–8 min, $n = 3$ or 4 slices; Fig. 8*B* and *C*), but not with AP5 ($100\,\mu$M, 8 min, $n = 3$ slices; Fig. 8*D*), reversibly abolished subicular SRFPs. These observations are supportive of the idea that the subicular SRFPs are generated by network activities involving both glutamate AMPA and GABA-A synapses.

To control possible disturbances associated with surgical cuts and to further explore regional spread of subicular SRFPs, we obtained conventional coronal slices from the caudal brain (0.5 mm thickness, two slices per half brain, see Methods). These slices contained ventral subicular and EC areas but excluded CA2/CA3 areas (Fig. 9*A*), and were thus suitable for monitoring subicular–EC regional activities in relative isolation. In response to stimulation of CA1/subicular or peri-subicular areas, the field EPSPs of the EC deep layer were 0.17 ± 0.02 or 0.42 ± 0.18 mV ($n = 12$ or 4), respectively (Fig. 9*B*), indicating preserved subicular–EC synaptic connections in these coronal slices. Stable SRFPs were observed from the subicular area, and subicular SRFPs were often coherent with SRFPs in the EC deep layer (Fig. 9*C*). The mean frequencies of subicular and EC SRFPs were 1.26 ± 0.17 and 1.06 ± 0.14 Hz, respectively ($n = 12$). After a surgical cut (as indicated by a thick dashed line in Fig. 9*A*) that separated the subicular and EC recording sites, the subicular area could still exhibit SRFPs but regular rhythmic activity was absent in the isolated EC area ($n = 3$ slices, Fig. 9*C*). These observations are consistent with the data obtained from thick slices (Fig. 3*A*), further suggesting that SRFPs can originate from the subicular circuit and propagate to the EC area.

Discussion

Relevance of SRFPs to hippocampal EEG activities

The rodent hippocampus exhibits two types of intermingled EEG activities during slow wave sleep or awake immobility: irregular activities and sharp waves (O'Keefe & Nadel, 1978; Buzsáki *et al.* 1983, 2003). The irregular activities have rhythmic signals over a wide frequency range (0.5–25 Hz) and their dominant frequencies are 2–3 Hz as revealed by spectral analyses (Leung *et al.* 1982; Jarosiewicz *et al.* 2002;

Jarosiewicz & Skaggs, 2004*a*,*b*). The sharp waves have intermittent occurrence frequencies (0.01–0.5 Hz) and large amplitudes (up to 3 mV), and they are often superimposed with ~200 Hz oscillatory spike activities called ripples (Buzsáki, 1986; Suzuki & Smith, 1987; Buzsáki *et al.* 2003). Hippocampal EEG sharp waves and irregular activities spread to the subiculum and EC deep layer areas (Chrobak & Buzsáki, 1994; Anderson & O'Mara, 2003), and the underlying network activities are thought to be crucial for hippocampus-dependent memory processes (Siapas & Wilson, 1998; Sirota *et al.* 2003; Jarosiewicz & Skaggs, 2004*a*,*b*; Battaglia *et al.* 2004).

The SRFPs we observed *in vitro* share some common features with the EEG irregular activities. Firstly, the *in vitro* SRFPs encompass a wide frequency range of rhythmic signals (0.5–20 Hz) and have dominant

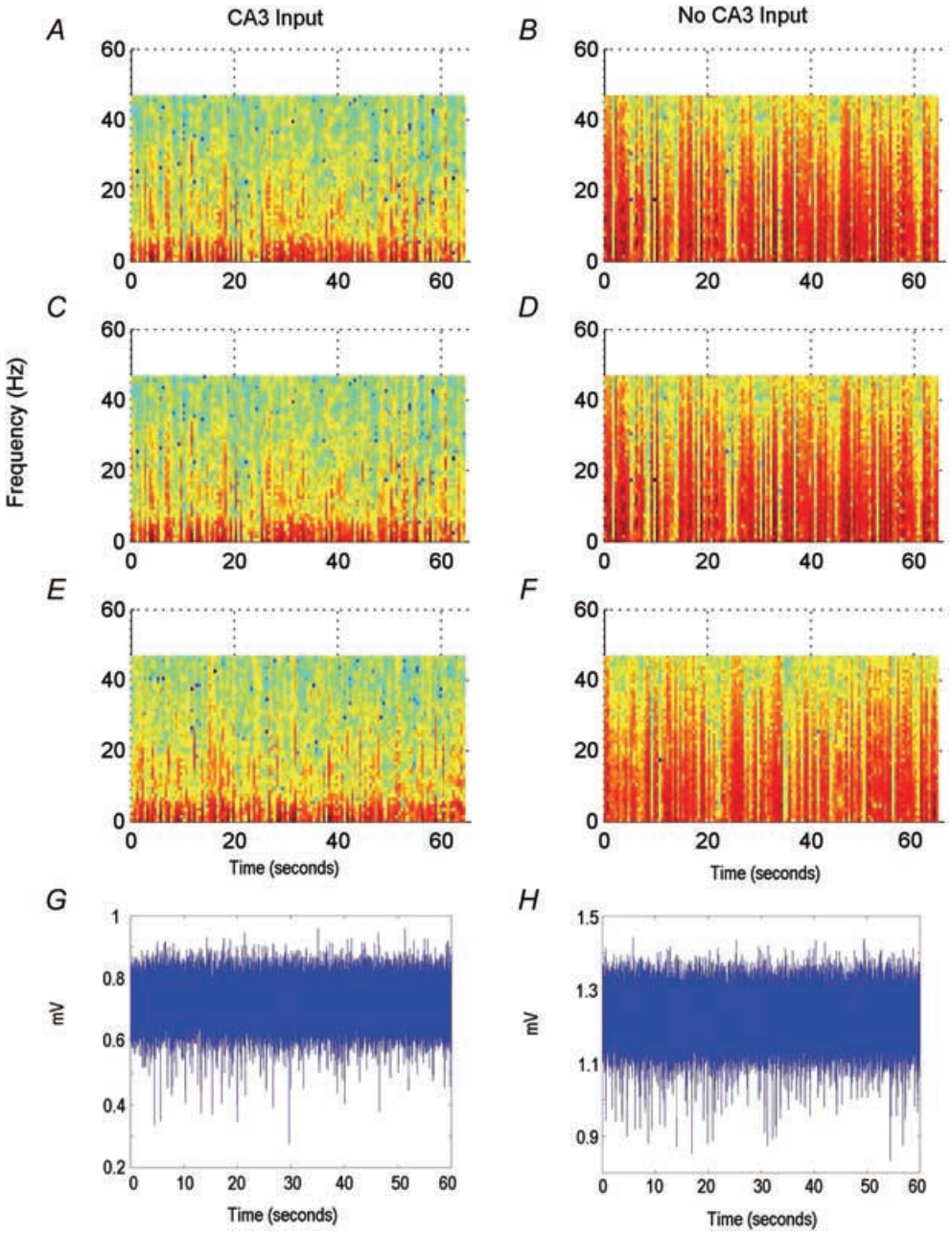

Figure 6. Spectrograms of subicular rhythms at 0.5 s resolution
Each spectrogram is from an individual slice. Amplitude is normalized with red representing high power to blue representing low power. *A*, *C* and *E*, rhythms taken from slices with CA3 input. *B*, *D* and *F*, rhythms taken from slices without CA3 input. *G* and *H*, unfiltered extracellular recording data of subicular rhythms used in *A* and *B*, respectively.

frequencies of 1–4 Hz (Wu *et al.* 2002, 2005*a*). Secondly, the SRFPs are often intermingled with an *in vitro* form of spontaneous sharp waves. The *in vitro* sharp waves are larger in amplitude (0.3–3 mV) and less frequent in occurrence (0.01–0.3 Hz) than the SRFPs. Distinct from the IPSP-based SRFPs, the *in vitro* sharp waves are correlated with coherent EPSPs/discharges in CA3 pyramidal neurons (Wu *et al.* 2005*b*). Thirdly, we show in the present experiments that the SRFPs can spread from CA3 to the subicular and EC areas (Fig. 3). Based on this information, we postulate that the network activities underlying SRFPs may participate in the generation of hippocampal EEG irregular activities.

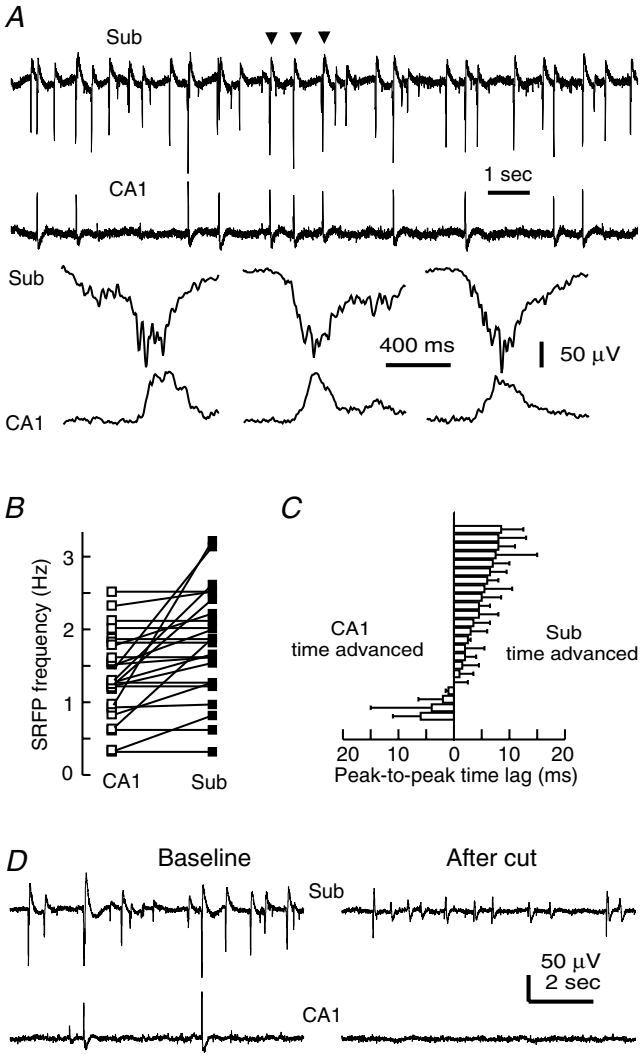

Figure 7. SRFPs observed from CA1–subicular miniature slices
A, representative extracellular traces were recorded simultaneously from the subicular and CA1 areas of a miniature slice. Arrows denoting SRFP events are shown in fast sweeps. *B*, frequencies of CA1 and subicular SRFPs were measured from 23 miniature slices. Data points represent mean frequencies calculated from ≥ 60 consecutive SRFP events in individual slices, and the frequencies of corresponding regional SRFPs are linked with continuous lines. *C*, peak-to-peak time lags of CA1 and subicular SRFPs were measured from ≥ 60 consecutive SRFP events; the mean time lags of individual slices are presented. *D*, representative traces were recorded from the subicular and CA1 areas of a miniature slice. A surgical cut was made after baseline recordings to separate the two recording sites. Note the absence of spontaneous field potentials in the isolated CA1 area after the cut.

Generation and regional spread of SRFPs

The CA3 recurrent circuit is known to play a prominent role in the generation of synchronous neuronal activities (Miles & Wong, 1986; Traub *et al.* 1989). The discharges of individual CA3 pyramidal neurons have been shown to effectively and preferentially excite local GABAergic inhibitory interneurons (Miles, 1990; Cohen & Miles, 2000; Fricker & Miles, 2000). We have shown in previous studies that the SRFPs originate from the CA3 area and that their intracellular correlates are characterized by synchronous GABA-A IPSPs in pyramidal neurons and repetitive discharges in inhibitory interneurons (Wu *et al.* 2002, 2005*a*). Based on this information, we have presented a hypothesis to account for SRFP generation and regional spread (Wu *et al.* 2005*a*). We propose that under standard *in vitro* conditions, sporadic discharges from a population of CA3 pyramidal neurons form a population excitatory drive which activates a group of GABAergic inhibitory interneurons. Once activated, the interneurons discharge rhythmically and coherently via mechanisms of mutual inhibition and gap junction couplings (Wang & Rinzel, 1993; Zhang *et al.* 1998; Skinner *et al.* 1999; Maier *et al.* 2003). The coherent interneuronal discharges then impose rhythmic IPSPs onto a large number of pyramidal neurons, which constitute a major ionic component of the SRFPs. We propose that the CA3 glutamate drive also excites CA1 interneurons via the Schaffer collateral pathway, thus mediating the local SRFPs in the CA1 area.

The SRFPs we observed from the isolated subicular circuit may be generated by similar mechanisms as proposed above. Harris *et al.* (2001) have shown that both regular spiking and burst firing pyramidal neurons of the rat subiculum have abundant interconnections, and the resulting excitatory activities can mediate synchronization and propagation of epileptiform discharges in the disinhibited subicular slices (Harris & Stewart, 2001*a*,*b*). Such pyramidal–pyramidal neuronal interconnections probably exist in the mouse subiculum. Moreover, because the 'packing density' of hippocampal neuronal elements is greater in mice than in rats (Insausti, 1993) and because the thick slices preserve a larger neuronal connectivity relative to the conventional slices, the interconnections of mouse subicular pyramidal neurons may form an excitatory drive which is sufficient to recruit local pyramidal neurons and inhibitory interneurons, and thereby to generate local SRFPs. The present observations that subicular SRFPs are

blocked by pharmacological antagonists of GABA-A or AMPA glutamate receptors are supportive of this view. Considering that a great proportion (~70% in our experiments) of subicular pyramidal neurons are burst firing neurons and that subicular SRFPs are correlated with mixed IPSPs/EPSPs in subicular pyramidal neurons, it is conceivable that the intrinsic network activities of the subicular circuit would have a high level of complexity. Such complexity may explain in part the persistent high-frequency (> 10 Hz) activities as revealed by spectrogram analyses of the SRFPs in CA1–subicular miniature slices (Fig. 6).

In 'intact' thick hippocampal–subicular–EC slices, although individually recorded CA1 pyramidal neurons barely show spontaneous discharges (Wu *et al.* 2002), it is possible that sparse discharges from a group of CA1 pyramidal neurons may be sufficient to influence the subicular networks and hence mediate the apparent spread of SRFPs from the CA1 to the subicular area. Previous morphological and electrophysiological studies have indicated that the axons of subicular pyramidal neurons project into the CA1 area (Berger *et al.* 1980; Köhler, 1985; Harris & Stewart, 2001*b*; Knopp *et al.* 2005). Such subicular–CA1 projections can induce excitatory responses in the CA1 pyramidal neurons (Commins *et al.* 2002; Shao & Dudek, 2005) and mediate the subicular–CA1 spread of epileptiform activities when examined in the presence of GABA-A receptor antagonists (Harris & Stewart, 2001*a*). It is conceivable that in the miniature CA1–subicular slices lacking CA3 inputs, the subicular–CA1 projections become dominant, thus spreading SRFPs from the subicular to the CA1 area.

Still, CA1 SRFPs can sometimes precede subicular SRFPs in the miniature CA1–subicular slices (Fig. 7*A*); the underlying mechanisms are unclear at present. One possibility is that the axon terminals of subicular pyramidal neurons synapse not only with CA1 pyramidal neurons but also with CA1 GABAergic inhibitory interneurons. As the

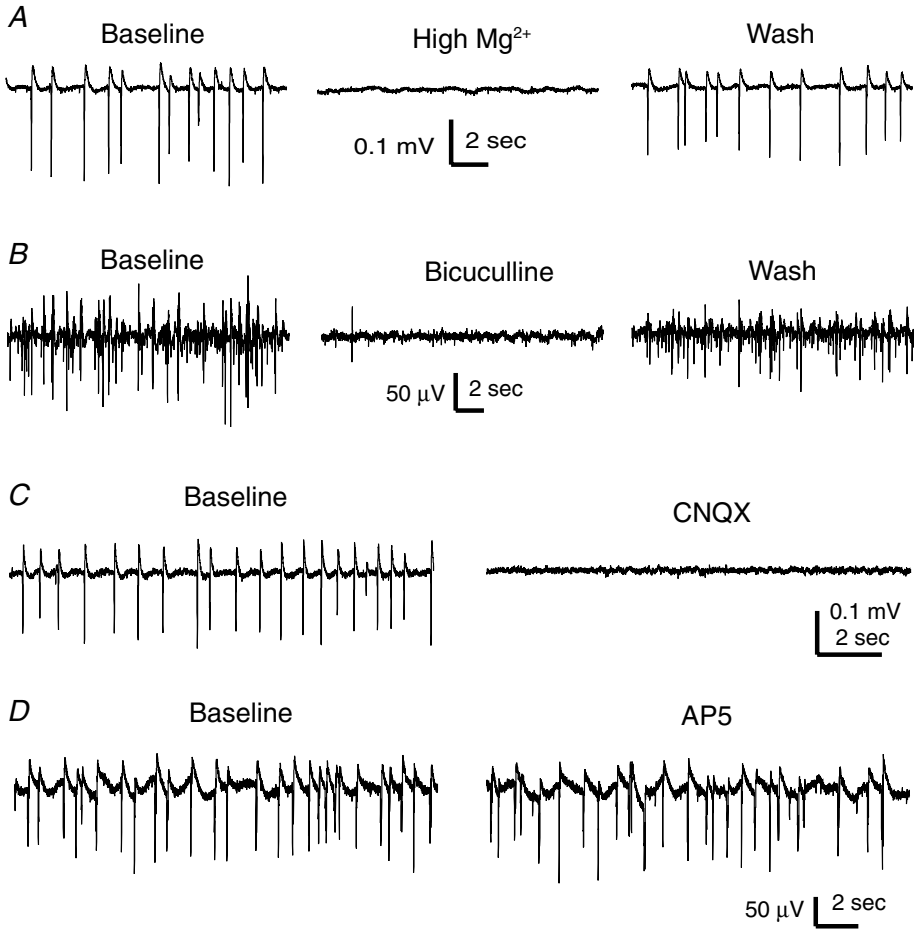

Figure 8. Pharmacological responses of subicular SRFPs
Extracellular traces were collected from the subicular area of four different miniature slices. *A*, subicular SRFPs were reversibly blocked by a high-Mg^{2+} ACSF (6 mM). *B–D*, bicuculline (10 μM), CNQX (10 μM) or AP5 (100 μM), respectively, was applied for 6–8 min, and traces were collected before and at the end of drug application.

CA1 SRFPs represent summed IPSPs from a large number of pyramidal neurons (Wu *et al.* 2002), the postulated innervation of CA1 interneurons by the subicular–CA1 projection, when effectively and preferentially activated (Miles, 1990; Cohen & Miles, 2000; Fricker & Miles, 2000), may promote the generation of CA1 SRFPs and hence partly account for the appearance of time advanced CA1 SRFPs in CA1–subicular miniature slices.

The mechanisms by which SRFPs are generated from the EC area remain to be examined. We show in the present experiments that a group of subicular pyramidal neurons, particularly the burst firing type, exhibit EPSPs/discharges in correlation with local SRFPs (Fig. 4), and that the EC SRFPs appear only in the deep layers which are the target of the axonal projection of subicular pyramidal neurons (Kloosterman *et al.* 2003). Moreover, the isolated EC area does not produce regular rhythmic activities (Figs 3 and 9). Based on these observations, we postulate that subicular inputs, especially the projection of burst firing subicular pyramidal neurons, are largely responsible for eliciting the EC SRFPs.

O'Mara *et al.* (2001) have postulated that the subiculum functions as an amplifier in hippocampal–cortical information transfer. In particular, subicular burst firing pyramidal neurons are thought to play an important role in the amplification of synaptic signals in both physiological and epileptiform activities. Our present data are supportive of this notion, suggesting that the subicular circuit serves as an amplifier to spread the SRFPs from the hippocampus proper to the EC. Specifically, we hypothesize that the discharges of subicular burst firing pyramidal neurons greatly promote excitatory activities in the subicular and EC circuits, probably via frequency-dependent facilitation or modulation of glutamate transmission (Silberberg *et al.* 2005), thus being crucial for the generation of subicular and EC SRFPs. To test this hypothesis, further experiments are needed to investigate how burst firing subicular pyramidal neurons interact among themselves and with other types of neurons in the subicular and EC areas.

Relevance of SRFPs to epileptiform activities

Schwartzkroin *et al.* (Schwartzkroin & Knowles, 1984; Schwartzkroin & Haglund, 1986) have examined spontaneous rhythmic activities of human temporal cortical neurons in brain slices that were obtained from surgical specimens of epileptic patients. Their data show

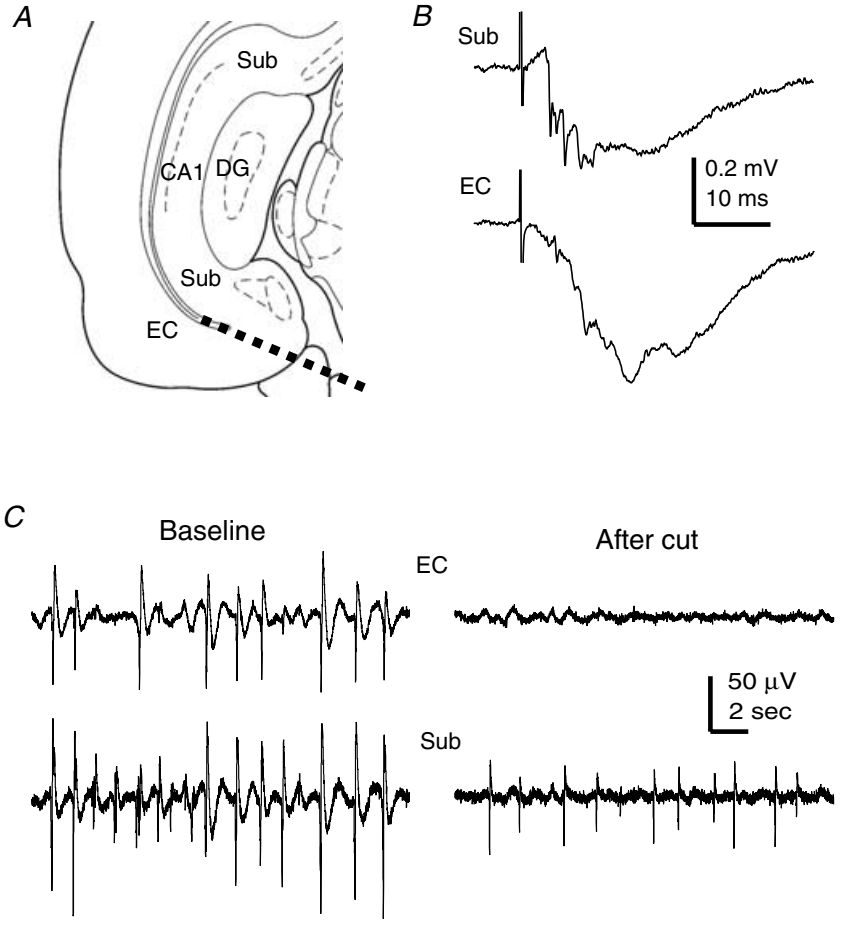

Figure 9. Subicular SRFPs observed from conventional coronal slices
A, a schematic illustration of CA1, subicular and EC areas in coronal brain slices. The thick dashed line denotes the position of a surgical cut used to separate the EC and subicular areas. *B*, subicular (top) and EC deep layer (bottom) field potentials were evoked by stimulation of the distal CA1 area. Illustrated traces were averaged from six consecutive responses. *C*, representative SRFPs were recorded simultaneously from the subicular and EC deep layer areas before (left) and after (right) a surgical cut that separated the two recording sites.

that rhythmic IPSPs of 2–4 Hz occur synchronously in pyramidal neurons, and that these IPSPs are blocked by GABA-A receptor antagonists and are correlated with discharges of local inhibitory interneurons. Because similar synchronous rhythmic IPSPs are also observed in pyramidal neurons of normal monkey hippocampal slices, it is hypothesized that these rhythmic IPSPs are non-epileptogenic in nature and result from the activity of local GABAergic interneurons. Köhling *et al.* (1998) and Straub *et al.* (2000) have observed similar spontaneous rhythmic activities in slices of temporal lobe tissues of epileptic patients. Their data show that ∼40% of these slices exhibit spontaneous rhythmic field potentials of 0.5–1 Hz. These spontaneous field rhythms are correlated largely with Cl^--dependent IPSPs in local pyramidal neurons and are blocked by pharmacological antagonists of GABA-A or AMPA glutamate receptors.

Cohen *et al.* (2002) have examined subicular neuronal activities in brain slices prepared form surgical specimens of epileptic patients. Their data show that the subicular circuit can exhibit spontaneous rhythmic activities of 0.5–3 Hz, which are thought to result from network activities involving both pyramidal neurons and GABAergic inhibitory interneurons. Cohen *et al.* (2003) have hypothesized that these rhythmic activities represent a form of epileptogenic plasticity as a consequence of sclerotic loss of CA3/CA1 pyramidal neurons. Wozny *et al.* (2003) have observed similar spontaneous rhythmic activities in subicular neurons of human epileptic temporal lobe tissues but suggested that such subicular rhythmic activities are not necessarily related to CA3/CA1 sclerosis.

Knopp *et al.* (2005) have examined subicular neuronal activities in horizontal slices (0.4 mm thickness) prepared from sham control rats and rats with pilocarpine-induced chronic seizures. Their data show that spontaneous rhythmic field potentials of 0.5–2 Hz occur frequently in the subicular area of pilocarpine-treated rat brain slices but not in controls (see Fig. 2*A* of Knopp *et al.* 2005). It is hypothesized that seizure-induced strengthening of synaptic contacts within the subicular recurrent network is responsible for the generation of such population rhythmic activities.

We show in the present study that the subicular circuit of non-seizure mice is capable of exhibiting SRFPs of 1–4 Hz *in vitro*. The manifestation of subicular SRFPs in the thick slices may be partly due to a better preservation of neuronal circuits in thick slices than in conventional slices and partly due to the greater 'packing density' of neuronal elements in the mouse hippocampus (Insausti, 1993). Our data suggest that the subicular SRFPs are not a consequence of experimentally induced disinhibition. We hypothesize, rather, that the ability to generate SRFPs is an intrinsic property of the mouse subicular circuit, and that the cellular and network machineries underlying the subicular SRFPs are highly sensitive to modulation by chronic seizures (Cohen *et al.* 2002; Wozny *et al.* 2003; Knopp *et al.* 2005). It would be of significant interest in future studies to isolate a relatively large subicular circuit from animals with chronic temporal lobe epilepsy and to examine seizure-induced alterations in subicular SRFPs.

References

Akay M (1997). Time-frequency and wavelets in biomedical signal processing. IEEE Press, New York.

Amaral DG & Witter MP (1989). The three-dimensional organization of the hippocampal formation: a review of anatomical data. *Neuroscience* **31**, 571–591.

Anderson MI & O'Mara SM (2003). Analysis of recordings of single-unit firing and population activity in the dorsal subiculum of unrestrained, freely moving rats. *J Neurophysiol* **90**, 655–665.

Anderton BH, Callahan L, Coleman P, Davies P, Flood D, Jicha GA, Ohm T & Weaver C (1998). Dendritic changes in Alzheimer's disease and factors that may underlie these changes. *Prog Neurobiol* **55**, 595–609.

Battaglia FP, Sutherland GR & McNaughton BL (2004). Hippocampal sharp wave bursts coincide with neocortical 'up-state' transitions. *Learn Mem* **11**, 697–704.

Behr J, Empson RM, Schmitz D, Gloveli T & Heinemann U (1996). Electrophysiological properties of rat subicular neurons in vitro. *Neurosci Lett* **220**, 41–44.

Benini R & Avoli M (2005). Rat subicular networks gate hippocampal output activity in an *in vitro* model of limbic seizures. *J Physiol* **566**, 885–900.

Berger TW, Swanson GW, Milner TA, Lynch GS & Thompson RF (1980). Reciprocal anatomical connections between hippocampus and subiculum in the rabbit evidence for subicular innervation of regio superior. *Brain Res* **183**, 265–276.

Buzsáki G (1986). Hippocampal sharp waves: their origin and significance. *Brain Res* **398**, 242–252.

Buzsáki G, Buhl DL, Harris KD, Csicsvari J, Czeh B & Morozov A (2003). Hippocampal network patterns of activity in the mouse. *Neuroscience* **116**, 201–211.

Buzsáki G, Leung LW & Vanderwolf CH (1983). Cellular bases of hippocampal EEG in the behaving rat. *Brain Res* **287**, 139–171.

Chrobak JJ & Buzsáki G (1994). Selective activation of deep layer (V-VI) retrohippocampal cortical neurons during hippocampal sharp waves in the behaving rat. *J Neurosci* **14**, 6160–6170.

Cohen I & Miles R (2000). Contributions of intrinsic and synaptic activities to the generation of neuronal discharges in *in vitro* hippocampus. *J Physiol* **524**, 485–502.

Cohen I, Navarro V, Clemenceau S, Baulac M & Miles R (2002). On the origin of interictal activity in human temporal lobe epilepsy in vitro. *Science* **298**, 1418–1421.

Cohen I, Navarro V, Le Duigou C & Miles R (2003). Mesial temporal lobe epilepsy: a pathological replay of developmental mechanisms? *Biol Cell* **95**, 329–333.

Colgin LL, Kubota D, Jia Y, Rex CS & Lynch G (2004). Long-term potentiation is impaired in rat hippocampal slices that produce spontaneous sharp waves. *J Physiol* **558**, 953–961.

Colling SB, Stanford IM, Traub RD & Jefferys JG (1998). Limbic gamma rhythms. I. Phase-locked oscillations in hippocampal CA1 and subiculum. *J Neurophysiol* **80**, 155–161.

Commins S, Aggleton JP & O'Mara SM (2002). Physiological evidence for a possible projection from dorsal subiculum to hippocampal area CA1. *Exp Brain Res* **146**, 155–160.

D'Antuono M, Kawasaki H, Palmieri C & Avoli M (2001). Network and intrinsic contributions to carbachol-induced oscillations in the rat subiculum. *J Neurophysiol* **86**, 1164–1178.

Deuchars J & Thomson AM (1996). CA1 pyramid-pyramid connections in rat hippocampus in vitro: dual intracellular recordings with biocytin filling. *Neuroscience* **74**, 1009–1018.

de Villers-Sidani E, Tahvildari B & Alonso A (2004). Synaptic activation patterns of the perirhinal-entorhinal inter-connections. *Neuroscience* **129**, 255–265.

Dhillon A & Jones RS (2000). Laminar differences in recurrent excitatory transmission in the rat entorhinal cortex *in vitro*. *Neuroscience* **99**, 413–422.

Dickson CT, Biella G & de Curtis M (2003). Slow periodic events and their transition to gamma oscillations in the entorhinal cortex of the isolated Guinea pig brain. *J Neurophysiol* **90**, 39–46.

Finch DM, Nowlin NL & Babb TL (1983). Demonstration of axonal projections of neurons in the rat hippocampus and subiculum by intracellular injection of HRP. *Brain Res* **271**, 201–216.

Finch DM, Tan AM & Isokawa-Akesson M (1988). Feed-forward inhibition of the rat entorhinal cortex and subicular complex. *J Neurosci* **8**, 2213–2226.

Flood DG (1991). Region-specific stability of dendritic extent in normal human aging and regression in Alzheimer's disease. II. Subiculum. *Brain Res* **540**, 83–95.

Fricker D & Miles R (2000). EPSP amplification and the precision of spike timing in hippocampal neurons. *Neuron* **28**, 559–569.

Funahashi M & Stewart M (1997). Presubicular and parasubicular cortical neurons of the rat: functional separation of deep and superficial neurons *in vitro*. *J Physiol* **501**, 387–403.

Gnatkovsky V & de Curtis M (2006). Hippocampus-mediated activation of superficial and deep layer neurons in the medial entorhinal cortex of the isolated guinea pig brain. *J Neurosci* **26**, 873–881.

Gray JA, Feldon J, Rawlins JNP, Hemsley DR & Smith AD (1991). The neuro-psychology of schizophrenia. *Behav Brain Sci* **14**, 1–84.

Greene JR (1996). Subiculum: a potential site of action for novel antipsychotic drugs? *Mol Psychiatry* **1**, 380–387.

Greene JR & Totterdell S (1997). Morphology and distribution of electrophysiologically defined classes of pyramidal and nonpyramidal neurons in rat ventral subiculum in vitro. *J Comp Neurol* **380**, 395–408.

Harris E & Stewart M (2001*a*). Propagation of synchronous epileptiform events from subiculum backward into area CA1 of rat brain slices. *Brain Res* **895**, 41–49.

Harris E & Stewart M (2001*b*). Intrinsic connectivity of the rat subiculum. II. Properties of synchronous spontaneous activity and a demonstration of multiple generator regions. *J Comp Neurol* **435**, 506–518.

Harris E, Witter MP, Weinstein G & Stewart M (2001). Intrinsic connectivity of the rat subiculum. I. Dendritic morphology and patterns of axonal arborization by pyramidal neurons. *J Comp Neurol* **435**, 490–505.

Harrison PJ (2004). The hippocampus in schizophrenia: a review of the neuropathological evidence and its pathophysiological implications. *Psychopharmacology (Berl)* **174**, 151–162.

Insausti R (1993). Comparative anatomy of the entorhinal cortex and hippocampus in mammals. *Hippocampus* **3**, 19–26.

Jarosiewicz B, McNaughton BL & Skaggs WE (2002). Hippocampal population activity during the small-amplitude irregular activity state in the rat. *J Neurosci* **22**, 1373–1384.

Jarosiewicz B & Skaggs WE (2004*a*). Hippocampal place cells are not controlled by visual input during the small irregular activity state in the rat. *J Neurosci* **24**, 5070–5077.

Jarosiewicz B & Skaggs WE (2004*b*). Level of arousal during the small irregular activity state in the rat hippocampal EEG. *J Neurophysiol* **91**, 2649–2657.

Jung HY, Staff NP & Spruston N (2001). Action potential bursting in subicular pyramidal neurons is driven by a calcium tail current. *J Neurosci* **21**, 3312–3321.

Kano T, Inaba Y & Avoli M (2005). Periodic oscillatory activity in parahippocampal slices maintained in vitro. *Neuroscience* **130**, 1041–1153.

Kapur J, Stringer JL & Lothman EW (1989). Evidence that repetitive seizures in the hippocampus cause a lasting reduction of GABAergic inhibition. *J Neurophysiol* **61**, 417–426.

Kloosterman F, Witter MP & Van Haeften T (2003). Topographical and laminar organization of subicular projections to the parahippocampal region of the rat. *J Comp Neurol* **455**, 156–171.

Knopp A, Kivi A, Wozny C, Heinemann U & Behr J (2005). Cellular and network properties of the subiculum in the pilocarpine model of temporal lobe epilepsy. *J Comp Neurol* **483**, 476–488.

Köhler C (1985). Intrinsic projections of the retrohippocampal region in the rat brain. I. The subicular complex. *J Comp Neurol* **236**, 504–522.

Köhling R, Lücke A, Straub H, Speckmann EJ, Tuxhorn I, Wolf P, Pannek H & Oppel F (1998). Spontaneous sharp waves in human neocortical slices excised from epileptic patients. *Brain* **121**, 1073–1087.

Kubota D, Colgin LL, Casale M, Brucher FA & Lynch G (2003). Endogenous waves in hippocampal slices. *J Neurophysiol* **89**, 81–89.

Lavenex P & Amaral DG (2000). Hippocampal–neocortical interaction: a hierarchy of associativity. *Hippocampus* **10**, 420–430.

Leung LS, Lopes Da Silva FH & Wadman WJ (1982). Spectral characteristics of the hippocampal EEG in the freely moving rat. *Electroencephalogr Clin Neurophysiol* **54**, 203–219.

Maier N, Güldenagel M, Söhl G, Siegmund H, Willecke K & Draguhn A (2002). Reduction of high-frequency network oscillations (ripples) and pathological network discharges in hippocampal slices from connexin 36-deficient mice. *J Physiol* **541**, 521–528.

Maier N, Nimmrich V & Draguhn A (2003). Cellular and network mechanisms underlying spontaneous sharp wave-ripple complexes in mouse hippocampal slices. *J Physiol* **550**, 873–887.

Mason A (1993). Electrophysiology and burst-firing of rat subicular pyramidal neurons in *vitro*: a comparison with area CA1. *Brain Res* **600**, 174–178.

Mattia D, Kawasaki H & Avoli M (1997). In vitro electrophysiology of rat subicular bursting neurons. *Hippocampus* **7**, 48–57.

Menendez de la Prida L (2003). Control of bursting by local inhibition in the rat subiculum *in vitro*. *J Physiol* **549**, 219–230.

Menendez de la Prida L & Gal B (2004). Synaptic contributions to focal and widespread spatiotemporal dynamics in the isolated rat subiculum in vitro. *J Neurosci* **24**, 5525–5536.

Menendez de la Prida L, Suarez F & Pozo MA (2003). Electrophysiological and morphological diversity of neurons from the rat subicular complex in vitro. *Hippocampus* **13**, 728–744.

Miles R (1990). Synaptic excitation of inhibitory cells by single CA3 hippocampal pyramidal cells of the guinea-pig *in vitro*. *J Physiol* **428**, 61–77.

Miles R & Wong RKS (1986). Excitatory synaptic interactions between CA3 neurones in the guinea-pig hippocampus. *J Physiol* **373**, 397–418.

Naber PA, Witter MP & Lopes Silva FH (2000). Networks of the hippocampal memory system of the rat. The pivotal role of the subiculum. *Ann NY Acad Sci* **911**, 392–403.

O'Keefe JA & Nadel L (1978). The hippocampus as a cognitive map. *Clarendon*. Oxford Press

O'Mara S (2005). The subiculum: what it does, what it might do, and what neuroanatomy has yet to tell us. *J Anat* **207**, 271–282.

O'Mara SM, Commins S, Anderson M & Gigg J (2001). The subiculum: a review of form, physiology and function. *Prog Neurobiol* **64**, 129–155.

Papatheodoropoulos C & Kostopoulos G (2002). Spontaneous GABA(A)-dependent synchronous periodic activity in adult rat ventral hippocampal slices. *Neurosci Lett* **319**, 17–20.

Schmitz D, Gloveli T, Behr J, Dugladze T & Heinemann U (1998). Subthreshold membrane potential oscillations in neurons of deep layers of the entorhinal cortex. *Neuroscience* **85**, 999–1004.

Schwartzkroin PA & Haglund MM (1986). Spontaneous rhythmic synchronous activity in epileptic human and normal monkey temporal lobe. *Epilepsia* **27**, 523–533.

Schwartzkroin PA & Knowles WD (1984). Intracellular study of human epileptic cortex: in vitro maintenance of epileptiform activity? *Science* **223**, 709–712.

Shao LR & Dudek FE (2005). Electrophysiological evidence using focal flash photolysis of caged glutamate that CA1 pyramidal cells receive excitatory synaptic input from the subiculum. *J Neurophysiol* **93**, 3007–3011.

Siapas AG & Wilson MA (1998). Coordinated interactions between hippocampal ripples and cortical spindles during slow-wave sleep. *Neuron* **21**, 1123–1128.

Silberberg G, Grillner S, LeBeau FE, Maex R & Markram H (2005). Synaptic pathways in neural microcircuits. *Trends Neurosci* **28**, 541–551.

Sirota A, Csicsvari J, Buhl D & Buzsáki G (2003). Communication between neocortex and hippocampus during sleep in rodents. *Proc Natl Acad Sci U S A* **100**, 2065–2069.

Skinner FK, Zhang L, Velazquez JL & Carlen PL (1999). Bursting in inhibitory interneuronal networks: a role for gap-junctional coupling. *J Neurophysiol* **81**, 1274–1283.

Squire LR, Stark CE & Clark RE (2004). The medial temporal lobe. *Annu Rev Neurosci* **27**, 279–306.

Staff NP, Jung HY, Thiagarajan T, Yao M & Spruston N (2000). Resting and active properties of pyramidal neurons in subiculum and CA1 of rat hippocampus. *J Neurophysiol* **84**, 2398–2408.

Stewart M & Wong RK (1993). Intrinsic properties and evoked responses of guinea pig subicular neurons in vitro. *J Neurophysiol* **70**, 232–245.

Straub H, Hohling JM, Kohling R, Lucke A, Tuxhorn I, Ebner A, Wolf P, Pannek H, Oppel F & Speckmann EJ (2000). Effects of nifedipine on rhythmic synchronous activity of human neocortical slices. *Neuroscience* **100**, 445–452.

Suzuki SS & Smith GL (1987). Spontaneous EEG spikes in the normal hippocampus. I. Behavioral correlates, laminar profiles and bilateral synchrony. *Electroencephalogr Clin Neurophysiol* **67**, 348–359.

Traub RD, Miles R & Wong RKS (1989). Model of the origin of rhythmic population oscillations in the hippocampal slice. *Science* **242**, 1319–1325.

Wang XJ & Rinzel J (1993). Spindle rhythmicity in the reticularis thalami nucleus: synchronization among mutually inhibitory neurons. *Neuroscience* **53**, 899–904.

Wong T, Zhang XL, Asl MN, Wu CP, Carlen PL & Zhang L (2005). Postnatal development of intrinsic GABAergic rhythms in mouse hippocampus. *Neuroscience* **134**, 107–120.

Wozny C, Kivi A, Lehmann TN, Dehnicke C, Heinemann U & Behr J (2003). Comment on 'On the origin of interictal activity in human temporal lobe epilepsy in vitro'. *Science* **301**, 463.

Wu C, Asl MN, Gillis J, Skinner FK & Zhang L (2005*a*). An in vitro model of hippocampal sharp waves: regional initiation and intracellular correlates. *J Neurophysiol* **94**, 741–753.

Wu C, Luk WP, Gillis J, Skinner F & Zhang L (2005*b*). Size does matter: generation of intrinsic network rhythms in thick mouse hippocampal slices. *J Neurophysiol* **93**, 2302–2317.

Wu C, Shen H, Luk WP & Zhang L (2002). A fundamental oscillatory state of isolated rodent hippocampus. *J Physiol* **540**, 509–527.

Zhang L, Huang H, Wu CP, Nassiri M, Wong T, Gillis J & Skinner FK (2005). Spontaneous population rhythmic activities of mouse subiculum in thick slices. *Program No. 970.3 2005 Abstract Viewer/Itinerary Planner Washington DC*. Society for Neuroscience Online.

Zhang L, Pennefather P, Velumian A, Tymianski M, Charlton M & Carlen PL (1995). Potentiation of a slow Ca^{2+}-dependent K^+ current by intracellular Ca^{2+} chelators in hippocampal CA1 neurons of rat brain slices. *J Neurophysiol* **74**, 2225–2241.

Zhang L, Spigelman I & Carlen PL (1991). Development of GABA-mediated, chloride-dependent inhibition in CA1 pyramidal neurones of immature rat hippocampal slices. *J Physiol* **444**, 25–49.

Zhang L, Weiner JL, Valiante TA, Velumian AA, Watson PL, Jahromi SS, Schertzer S, Pennefather P & Carlen PL (1994). Whole-cell recording of the Ca^{2+}-dependent slow afterhyperpolarization in hippocampal neurones: effects of internally applied anions. *Pflugers Arch* **426**, 247–253.

Zhang Y, Perez-Velazquez JL, Tian GF, Wu CP, Skinner FK, Carlen PL & Zhang L (1998). Slow oscillations ($\leq$1 Hz) mediated by GABAergic interneuronal networks. *J Neurosci* **18**, 9256–9268.

Acknowledgements

This work was supported by research grants from the Canadian Institutes of Health Research (CIHR MOP-44092 to L.Z.) and the Natural Sciences and Engineering Research Council of Canada (NSERC to F.K.S. and L.Z.), and a CIHR Doctoral Award with Epilepsy Canada (to J.G.). The authors thank Ms Alice Hsu and Mr Xiaodi Wu for critical reading of this manuscript.

Author's present address

M. Nassiri Asl: Department of Pharmacology, Faculty of Medicine, Qazvin University of Medical Sciences, Iran.